ACS SENSORS

pubs.acs.org/acssensors

Article

Dual-Modality Detection of Early-Stage Drug-Induced Acute Kidney Injury by an Activatable Probe

Lingyan Liu, Liping Jiang, Wei Yuan, Zhongkuan Liu, Dongya Liu, Peng Wei,* Xinyu Zhang, and Tao Yi*

Cite This: *ACS Sens.* 2020, 5, 2457−2466

Read Online

ACCESS | Metrics & More | Article Recommendations | Supporting Information

ABSTRACT: Early detection of drug-induced acute kidney injury (AKI) is crucial for effective treatment and prevention of further injury. It remains challenging, however, because of the lack of activatable indicators with multimodality imaging capability that could increase the accuracy of diagnosis by mutual verification. Herein, we report an activatable probe, **FDOCl-22**, that enabled dual-modality detection of the early-stage drug-induced AKI. **FDOCl-22** was completely soluble in water and highly sensitive to hypochlorous acid (HOCl). Dramatic increases of both near-infrared (NIR) emission and absorption were observed after reaction with HOCl. A correlation between HOCl concentration and drug-induced AKI was established using **FDOCl-22** as a tool. As a consequence, the HOCl-activated probe was able to detect the early-stage drug-induced AKI by dual-modality imaging, irrespective of the drug stimulation time or dosage, by combining NIR fluorescence and photoacoustic imaging.

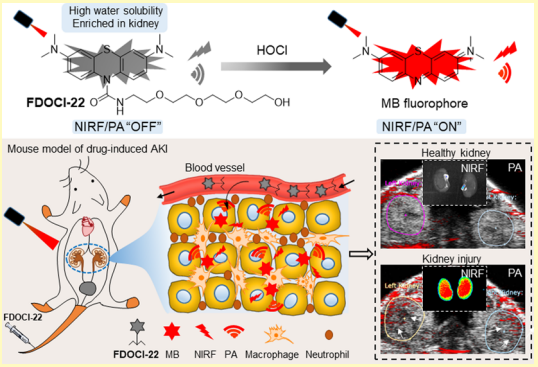

KEYWORDS: *activatable fluorescent probe, biosensor, dual-modality imaging, early detection, drug-induced acute kidney injury*

The kidney, one of the most important organs in the body, plays an essential role in the clearance of endogenous waste substances and xenobiotics.[1] It is, however, vulnerable to injury by commonly used drugs. Acute kidney injury (AKI) is a common but serious clinical disease that is associated with high morbidity and mortality.[2−5] In an epidemiological survey, drug-induced AKI accounted for about 30% of AKI clinical cases.[6] The commonly used methods for clinical detection of AKI, including routine blood examination (serum creatinine (CREA) and blood urea nitrogen (BUN)), do not easily identify early-stage AKI.[7,8] Indeed, irreversible damage may have occurred before the disease is diagnosed. Therefore, early detection of drug-induced AKI is necessary for the effective prevention of kidney damage and the treatment of the disease.

Cisplatin (dichlorodiamino platinum), a widely used universal agent for cancer treatment, has been proven to cause severe kidney injury.[9] Although the pathophysiological mechanisms of drug-induced AKI are multifactorial, some studies have shown that cisplatin-induced AKI may be due to cell apoptosis and inflammation caused by oxidative stress.[10−12] This suggests that direct detection of reactive oxygen species (ROS), produced during oxidative stress, may be a good strategy for the identification of early-stage drug-induced AKI. In fact, there have been several excellent attempts to diagnose related diseases using ROS-activated probes in recent years. These activatable probes have advantages that include low background noise and real-time detection.[13−21] Especially, Pu et al. have recently exploited a series of molecular fluorescence/chemiluminescence probes with high renal clearance efficiency for detecting disease biomarkers in kidney injury.[22−25] Zhang et al. first tracked fluctuations of $O_2^{\bullet-}$ levels during drug-induced AKI and then visualized fluctuations of endogenous hypochlorous acid (HOCl) resulting from drug-induced acute nephrotoxicity.[26,27] These studies indicated that the identification of a specific ROS could be an important breakthrough for the detection of early-stage drug-induced AKI.

Activatable probes that combine fluorescence imaging with other imaging modalities are needed for a precise diagnosis of drug-induced AKI since mutually noninterfering imaging methods can improve the accuracy of early detection.[28] However, the recently reported activatable probes for the diagnosis of drug-induced AKI are limited by their reliance on fluorescence as the only readout. There is therefore an urgent need to develop probes that combine multiple imaging modalities to achieve detection of early-stage drug-induced AKI.

Received: March 30, 2020
Accepted: July 24, 2020
Published: July 24, 2020

https://dx.doi.org/10.1021/acssensors.0c00640
ACS Sens. 2020, 5, 2457−2466

Scheme 1. Strategy of Designing Probes[a]

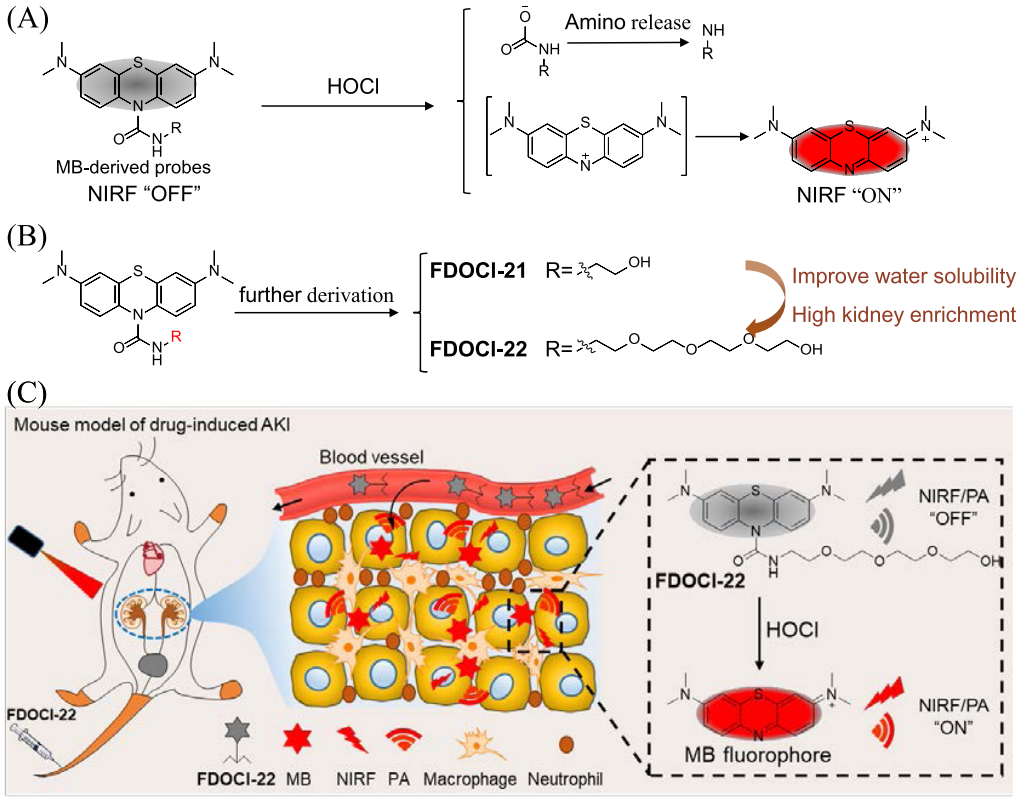

[a](A) Reaction mechanism of HOCl activatable fluorescent probes. (B) Structural modification and (C) diagrammatic sketch of dual-modality detection of early-stage drug-induced AKI in this work.

We have invested much effort in the development of fluorescent probes for several years, especially ROS-related probes.[29−35] In recent work, we successfully developed a series of activatable fluorescent probes using methylene blue (MB) as the fluorophore.[36] It was also reported that MB was a good reagent for photoacoustic (PA) imaging.[37,38] The advantages of PA imaging include increased penetration depth and spatial resolution *in vivo*.[39,40] In this report, we designed and synthesized two HOCl-activated probes, **FDOCI-21** and **FDOCI-22**, through structural modification based on our previous work (Scheme 1). **FDOCI-22** was completely soluble in water and showed remarkable near-infrared (NIR) emission and absorption changes upon the addition of HOCl, with high selectivity and sensitivity. Using **FDOCI-22**, we found that the level of HOCl was closely correlated with drug-induced AKI. Moreover, **FDOCI-22** could be used as a tool to detect early-stage drug-induced AKI and to assess the extent of drug-induced AKI by combining NIR fluorescence (NIRF) and PA imaging.

RESULTS AND DISCUSSION

Design of the Probes. Because the aim was to build HOCl-activated probes with dual fluorescence and photoacoustic imaging capability, the fluorophore was required to exhibit dramatic changes of both NIR emission and absorption. Recently, we have developed a platform for building functional fluorescent probes based on the MB fluorophore by switching between MB and LMB (leucomethylene blue, caged MB).[36] In the presence of HOCl, probes derived from this platform release MB fluorophore that is accompanied by remarkable changes in NIR emission and absorption (Scheme 1A). This platform was therefore suitable for designing our desired probe. Additionally, there have been literature reports that compounds with high water solubility are more likely to be enriched in the kidney.[41,42]

Two new probes, **FDOCI-21** and **FDOCI-22**, were designed and synthesized using our reported platform, incorporating hydrophilic groups to enhance water solubility (Scheme 1B). The synthetic details and characterization of these probes are provided in the Supporting Information. Their structures were confirmed by nuclear magnetic resonance (NMR) spectroscopy and high-resolution mass spectrometry (HRMS) as shown in Figures S1−S6 in the Supporting Information. Fortunately, **FDOCI-22**, which contained a longer ethylene glycol chain, was completely soluble in water without requiring any organic cosolvent (Table S1). Therefore, **FDOCI-22** is an ideal probe for further biological application.

Spectral Response of the Probes to HOCl. The stock solution of **FDOCI-22** (1 mM) was prepared in pure deionized water, while the dissolution of the analogue containing a shorter ethylene glycol chain (**FDOCI-21**) required the addition of ethanol as a cosolvent (details are provided in the Supporting Information). The response of the probes to HOCl *in vitro* was studied by spectroscopy under simulated physiological conditions (10 mM phosphate-buffered saline (PBS), pH 7.4). As shown in Figure 1A, the fluorescence intensity of **FDOCI-22** in the range of 640−800 nm increased dramatically upon addition of different concentrations of HOCl. The absorption of **FDOCI-22** in the range of 550−700 nm also increased remarkably, with a maximum absorbance at 664 nm after the addition of 10 μM HOCl (80-fold increase;

https://dx.doi.org/10.1021/acssensors.0c00640
ACS Sens. 2020, 5, 2457−2466

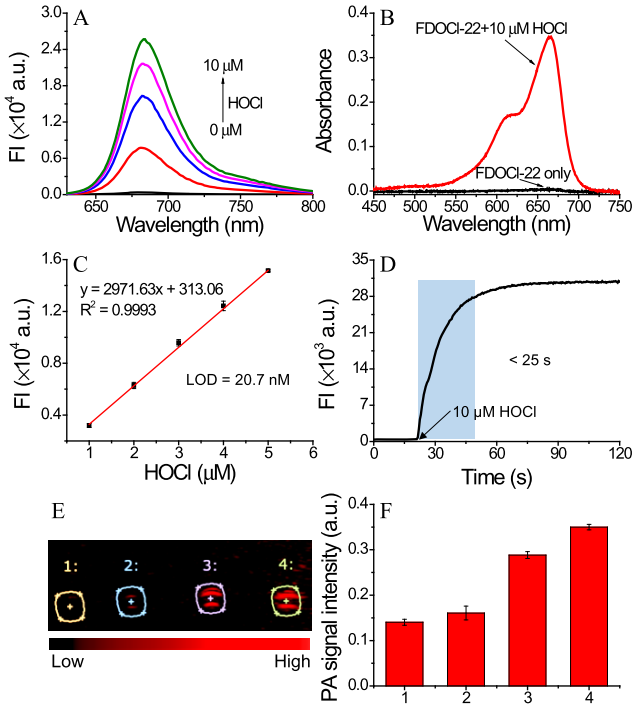

Figure 1. (A) Fluorescence spectra of **FDOCl-22** (5 μM in 10 mM PBS, pH 7.4) in the presence of different concentrations of HOCl (0, 2, 5, 7, and 10 μM). (B) Absorption spectra of **FDOCl-22** (5 μM in 10 mM PBS, pH 7.4) before and after adding HOCl (10 μM). (C) Fluorescence intensity of **FDOCl-22** (5 μM in 10 mM PBS, pH 7.4) with different concentrations of HOCl (1, 2, 3, 4, and 5 μM) at 686 nm. (D) Time-dependent changes in the fluorescence intensity of **FDOCl-22** (5 μM) at 686 nm after adding HOCl (10 μM) (λ_{ex} = 620 nm). (E) Photoacoustic images of **FDOCl-22** aqueous solution (1: PBS buffer; 2: 50 μM **FDOCl-22** with 100 μM HOCl; 3: 100 μM **FDOCl-22** with 200 μM HOCl; 4: 150 μM **FDOCl-22** with 300 μM HOCl). (F) Quantification of PA signal intensity in (E) (λ_{ex} = 680 nm).

Figure 1B), indicating the formation of the MB fluorophore (further confirmed by HRMS and high-performance liquid chromatography (HPLC) analysis; see Figures S7 and S8). The detection limit of the **FDOCl-22** response to HOCl was 20.7 nM based on the $3\sigma/k$ method (Figure 1C). In addition, the response time of the probe to HOCl was <25 s (Figure 1D). The response of **FDOCl-22** to HOCl was comparable to those of **FDOCl-21** and our reported probes (Figure S9). These data illustrated that the enhancement of water solubility did not affect the performance of the probe (Table S1). **FDOCl-22** maintained high sensitivity to HOCl in aqueous media compared with similar probes.

The selectivities of **FDOCl-21** (5 μM) and **FDOCl-22** (5 μM) toward HOCl were then determined by evaluating fluorescence intensity and absorbance changes before and after the addition of HOCl or other ROS/reactive nitrogen species (RNS). As shown in Figures S10 and S11, even high concentrations of ROS/RNS (H_2O_2, TBHP, NO, $^{\bullet}OH$, O_2^{-}, $ROO^{\bullet}$, t-$BuOO^{\bullet}$, and $ONOO^{-}$, 20 μM, 4 equiv) did not cause obvious changes of fluorescence intensity or absorbance. Remarkably, of the tested substances, only HOCl induced a significant enhancement of fluorescence and absorption. Although the reactions between amides and $^{\bullet}OH$ were reported, most of those reactions are structure-dependent and required harsh reaction conditions, such as hot alkali, high temperature, enzymes, and strong acidic conditions.[43] In the present work, the insensitivity of **FDOCl-21** (5 μM) and **FDOCl-22** toward $^{\bullet}OH$ may be because the experimental conditions that mimic the normal physiological conditions do not meet the requirements of harsh condition for the reaction between $^{\bullet}OH$ and amide. Indeed, in the reported $^{\bullet}OH$ probes containing amide groups, the amide was not the reaction site.[29,44] Moreover, singlet oxygen ($^1O_2$) will not interfere with the response of probe **FDOCl-22** toward **HOCl** (Figures S12 and S13). These results indicated that the probes had good selectivity for HOCl.

For broader biological applications, the impact of pH on the detection of HOCl by the probes was evaluated. As shown in Figure S14, the change in fluorescence intensity of the probes induced by 10 μM HOCl (2 equiv) was constant in the range of pH 3−10. Moreover, the stability of **FDOCl-22** in different buffers, nutrient solution, and urine was evaluated over various times (Figure S15). No significant changes in fluorescence of **FDOCl-22** (5 μM) were observed, even after 12 h in these media, indicating that **FDOCl-22** was sufficiently stable in physiological environments. These results demonstrated that **FDOCl-22** could be used for the detection of HOCl in a wide variety of physiological environments.

Because the absorption by **FDOCl-22** in response to HOCl exhibited remarkable changes in the range of 550−700 nm, the PA signals of **FDOCl-22** solutions (0, 50, 100, and 150 μM) incubated with different concentrations of HOCl were then measured using a light source at 680 nm. As expected, the PA signals were enhanced as the **FDOCl-22** concentration was increased (Figure 1E,F). The results indicated that the HOCl-activated probe, **FDOCl-22**, was capable of dual-modality fluorescence and photoacoustic imaging.

Fluorescence Imaging of HOCl in Cisplatin-Induced Apoptosis Using FDOCl-22. Oxidative stress, which is accompanied by increased ROS, has been proven to be a major contributory mechanism in the pathogenesis of drug-induced renal injury.[45−47] To further understand the pathology of cisplatin-induced AKI, we used our probe with a specific cell model to explore whether HOCl was produced during drug-induced apoptosis. Macrophages were selected as the model cells because they can sense tissue damage and induce innate immunity. These cells are an important source of many cytokines that have been identified as drivers of inflammation.[48]

Apoptosis was stimulated using cisplatin at different concentrations for various time periods and monitored by flow cytometry. As shown in Figure 2A (a1−a3), when RAW264.7 cells were exposed to 500 and 1000 μM cisplatin for 5 h, the number of apoptotic cells increased to 26.2 and 42.5%, respectively, compared with 2.2% in the negative control group. After incubation with 500 and 1000 μM cisplatin for 10 h, apoptosis increased to 71.5% (69.1% early apoptotic cells) and 76.8% (73.8% late apoptotic cells), respectively (Figure 2A, a4,a5). This confirms that cisplatin-induced apoptosis in a dose-dependent manner.

There is extensive evidence for the role of HOCl in apoptosis.[49−52] The correlation between HOCl concentration and apoptosis was therefore evaluated by flow cytometry and confocal laser scanning microscopy (CLSM). As shown in Figure 2A (a6), when RAW264.7 cells were exposed to 100 μM HOCl for 15 min, more than 45% of the cells were apoptotic, so this system could be selected as an apoptosis model. The production of HOCl during cisplatin-induced

https://dx.doi.org/10.1021/acssensors.0c00640
ACS Sens. 2020, 5, 2457−2466

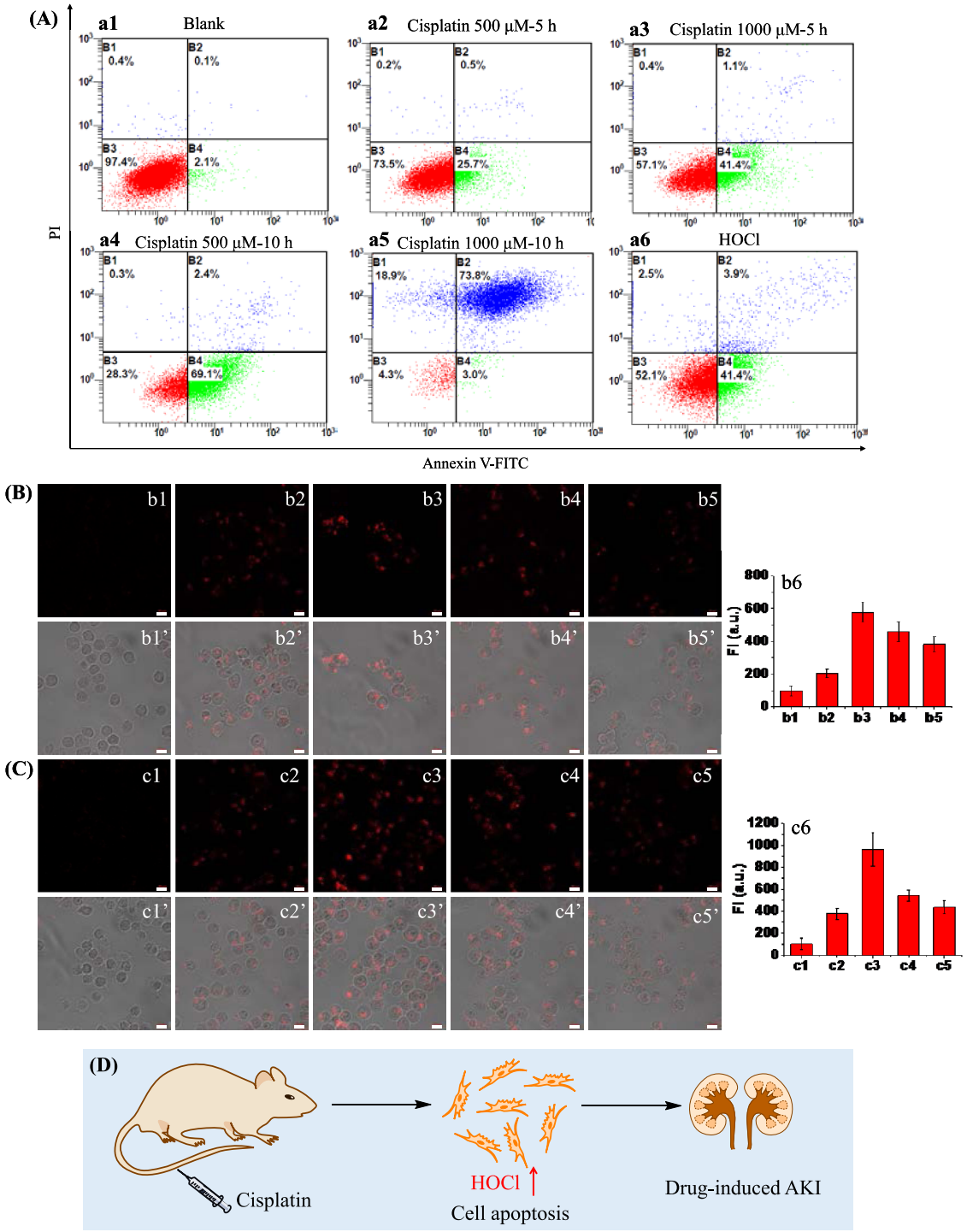

Figure 2. (A) RAW264.7 cell distributions with Annexin V-FITC/PI uptake measured by flow cytometer. (a1) Cells without any stimulation; (a2) with 500 μM cisplatin for 5 h; (a3) 1000 μM cisplatin for 5 h; (a4) 500 μM cisplatin for 10 h; (a5) 1000 μM cisplatin for 10 h; cisplatin is in serum-free medium; (a6) cells incubated with 100 μM HOCl in PBS (pH 7.4) for 15 min (B1: dead cells, Annexin V negative/PI positive; B2: late apoptotic cells, Annexin V positive/PI positive B3: living cells, Annexin V negative/PI negative; B4: early apoptotic cells, Annexin V positive/PI negative). Numbers in the respective quadrant profiles indicate the percentage of the cells present in this area. CLSM images of live RAW264.7 cells prestimulated with cisplatin for (B) 5 h and (C) 10 h and then treated with 10 μM **FDOCl-22** (cells were treated with b1, b1′, c1, c1′: **FDOCl-22** only; b2, b2′, c2, c2′: 500 μM cisplatin; b3, b3′, c3, c3′: 1000 μM cisplatin; b4, b4′, c4, c4′: preincubated with LC (500 μM) and b5, b5′, c5, c5′: LC (1000 μM) in the presence of 1000 μM cisplatin); b1′−b5′ and c1′−c5′ are merged images of b1−b5 and c1−c5 with bright field, respectively; (b6) and (c6) histograms presenting the average fluorescence intensity in (B) and (C), respectively. Scale bar = 10 μm. (D) Schematic illustration of cisplatin-induced AKI.

apoptosis was then studied using **FDOCl-22** by CLSM. As shown in Figures 2B,C (b1,b1′, and c1,c1′, respectively), RAW264.7 cells incubated with 10 μM **FDOCl-22** alone for 30 min showed no fluorescence signal. The fluorescence dose-dependently increased significantly when the cells were preincubated with different concentrations of cisplatin (500

https://dx.doi.org/10.1021/acssensors.0c00640
ACS Sens. 2020, 5, 2457−2466

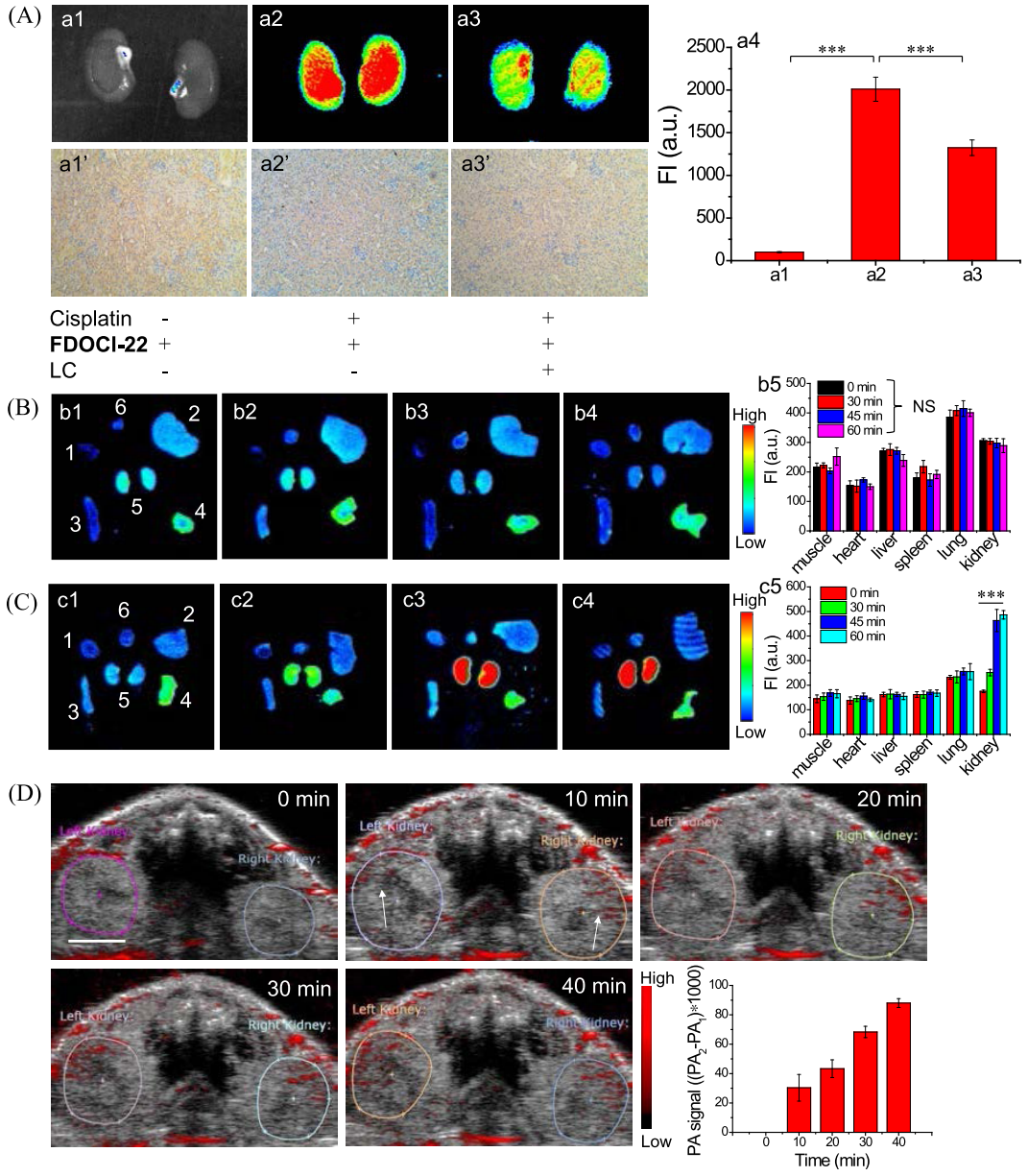

Figure 3. (A) Fluorescent imaging of kidney of mice (a1) only intravenously injected with **FDOCl-22** (200 μL × 0.5 mM) for 45 min; (a2) injected intraperitoneally with cisplatin (20 mg/kg) for 48 h and then intravenously injected with **FDOCl-22** (200 μL × 0.5 mM) for 45 min; (a3) pretreated with LC (500 mg/kg, 24 h) before injected intraperitoneally with cisplatin (20 mg/kg) for 48 h and then intravenously injected with **FDOCl-22** (200 μL × 0.5 mM) for 45 min; and (a4) average fluorescence intensity output of the group. (a1′−a3′) TNF-α staining images of kidney in panels (a1)−(a3). Values are the mean ± s.d. for n = 5. Fluorescent images of major organs of (B) healthy mouse and (C) AKI mouse model (injected intraperitoneally with cisplatin 20 mg/kg for 48 h) intravenously injected with **FDOCl-22** (200 μL × 0.5 mM) for different times (b1−b4 and c1−c4: 0, 30, 45, 60 min, respectively, and b5 and c5: average fluorescence intensity output of the group (1: heart, 2: liver, 3: spleen, 4: lung, 5: kidney)). (D) *In vivo* PA imaging of cisplatin-induced AKI mice (20 mg/kg, 48 h) in the kidney at different time points after intravenously injected with **FDOCl-22** (200 μL × 0.5 mM); the histogram is the PA intensity of kidneys at different time points (PA_2: PA intensity at different time points; PA_1: PA intensity at 0 min; n = 3 per group). Scale bar = 3 mm. Values are the mean ± s.d. for n = 5, ***p < 0.001. NS: not significant.

and 1000 μM) for 5 h and then treated with **FDOCl-22** for 30 min (Figure 2B, b2,b2′, and b3,b3′, respectively). When the preincubation time with cisplatin was increased (500 and 1000 μM for 10 h), the fluorescence intensity of **FDOCl-22** became much stronger than that after 5 h preincubation (Figure 2C, c2,c2′ and c3,c3′). To further verify the relationship between changes of fluorescence intensity and drug-induced AKI, L-carnitine (LC), an antioxidant that inhibits cisplatin-induced oxidative injury in cells,[53] was co-incubated with cisplatin (500 and 1000 μM). As shown in Figure 2B (b4,b4′, and b5,b5′) and 2C (c4,c4′ and c5,c5′), the fluorescence signal decreased as the concentration of LC was increased. Furthermore, we also detected HOCl produced by neutrophils stimulated by cisplatin. As shown in Figure S16, the fluorescence intensity dose-dependently increased significantly when the neutrophils were incubated with different concentrations of cisplatin (300, 500, and 1000 μM) for 2 h. These data demonstrated the production of HOCl during drug-induced apoptosis (Figure 2D). From the cell experiments, we could conclude that the production of HOCl during drug-induced apoptosis was

https://dx.doi.org/10.1021/acssensors.0c00640
ACS Sens. 2020, 5, 2457−2466

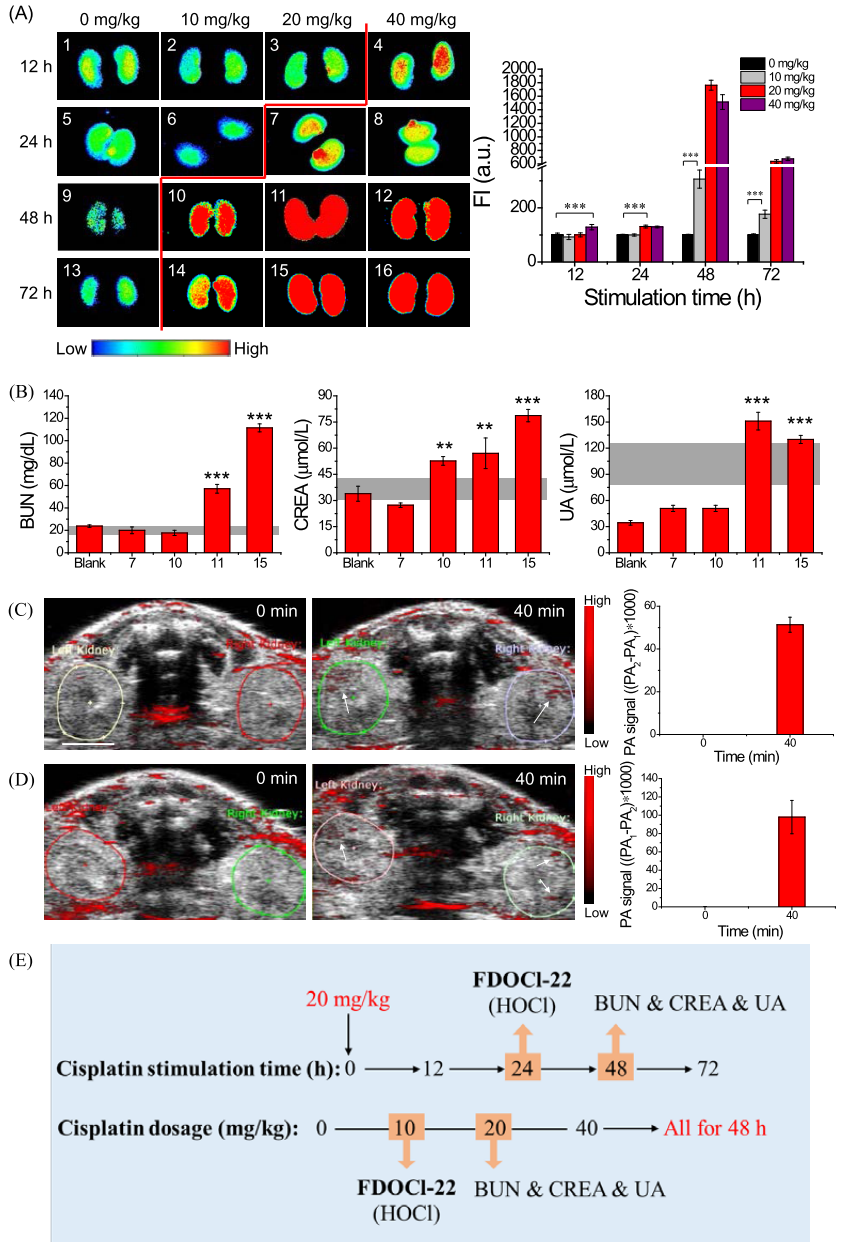

Figure 4. (A) Fluorescent images of the kidney of a series of mice intraperitoneally injected with cisplatin of varying concentrations (0, 10, 20, and 40 mg/kg) for different time periods (12, 24, 48, and 72 h) and then intravenously injected with **FDOCl-22** (200 μL × 0.5 mM) (left) and average fluorescence intensity output of the groups (right). (B) Changes in serum biomarkers of different models determined using commercial kits. These data are the mean ± s.d.; n = 3 independent experiments for BUN, CREA, and UA. The gray part indicates the normal fluctuation. *In vivo* PA imaging of cisplatin-induced AKI mice (C: 10 mg/kg, 48 h; D: 20 mg/kg, 24 h) in the kidney at 0 and 40 min after intravenously injected **FDOCl-22** (200 μL × 0.5 mM); the histogram is the corresponding PA intensity of kidneys at 0 and 40 min (PA_2: PA intensity at 40 min; PA_1: PA intensity at 0 min; n = 3 per group). (E) Schematic illustration of the detection timeline of **FDOCl-22** comparing clinical assay. Scale bar = 3 mm. $^{**}p$ <0.01, $^{***}p$ <0.001.

dependent on both dosage and injury time. Thus, HOCl may be used as a marker for the detection of early-stage drug-induced AKI.

Biocompatibility Studies of FDOCl-22. The biocompatibility of **FDOCl-22** was evaluated in cells and *in vivo*. The cytotoxicity of **FDOCl-22** toward RAW264.7 macrophages was determined using the cell counting kit-8 (CCK-8) assay. The results indicated that **FDOCl-22** had no toxic effects on RAW264.7 cells after 12 or 24 h of exposure (Figure S17). Additionally, the potential side effects of **FDOCl-22** were evaluated by serum biochemistry analysis and hematoxylin and eosin (H&E) staining assays. According to the H&E staining results, **FDOCl-22** did not induce any obvious pathological damage to major organs compared with the control group (Figure S18). Serum biochemical analysis in healthy mice indicated that their blood indexes were not significantly changed compared with the control group at 3 and 26 h after injection of **FDOCl-22** (Figure S19). Furthermore, renal function was not affected by **FDOCl-22** at 3 and 26 h after injection (Figure S20). All of the data confirm that **FDOCl-22** has good biocompatibility.

https://dx.doi.org/10.1021/acssensors.0c00640
ACS Sens. 2020, 5, 2457−2466

Dual-Modality Imaging of FDOCl-22 in a Mouse Model of Drug-Induced AKI. The excellent performance exhibited by **FDOCl-22** *in vitro* guarantees its application for the detection of drug-induced AKI *in vivo*. First, the *in vivo* distribution of **FDOCl-22** was studied. Healthy mice were injected with **FDOCl-22**, after which the main organs were harvested and incubated with HOCl (100 μM, 30 min) for fluorescence imaging. The fluorescence of these organs was compared with that of the control group (without **FDOCl-22**). A significant difference in fluorescence signal was only observed in the kidneys (Figure S21). According to the report of literature, the probe was most likely posited at kidney tubules rather than glomeruli because the tubules were at the frontline of clearance of nephrotoxin and vulnerable to be injured by commonly nephrotoxin exposure.[22,25] The results indicated that our design strategy was feasible and that the probe, **FDOCl-22**, was enriched in the kidney.

FDOCl-22 was then used to image cisplatin-induced AKI in a mouse model. Fluorescence changes in the kidney were tested at different times after injection of **FDOCl-22** (200 μL, 0.5 mM) through the tail vein of mice 48 h after intraperitoneal injection of cisplatin (20 mg/kg). As shown in Figure S22, the fluorescence intensity in the kidney increased time-dependently during 45 min and remained stable until 60 min. We, therefore, chose 45 min after injection via the tail vein for subsequent studies.

To verify that the fluorescence intensity changes were related to cisplatin-induced AKI, the effects of LC were evaluated *in vivo*. The kidneys of mice pretreated with cisplatin (20 mg/kg, 48 h), followed by intravenous injection of **FDOCl-22**, exhibited fluorescence enhancement compared to the control group. However, the fluorescence signal was decreased in the mice pretreated with LC (500 mg/kg) for 24 h before cisplatin treatment (Figure 3A: a1−a4). In addition, TNF-α immunostaining analysis indicated that the severity of kidney inflammation induced by cisplatin was significantly higher than that in healthy or LC pretreated mice (Figure 3A: a1′−a3′), which was consistent with the observed fluorescence intensity changes. Moreover, we also performed the IL-6 immunostaining of different models of mice and IL-6 overexpressed in kidney injury (Figure S23). These data illustrated that the fluorescence intensity changes of **FDOCl-22** were strongly correlated with cisplatin-induced AKI.

The biodistribution of **FDOCl-22** was further confirmed by comparison of the fluorescence images of healthy mice and the mouse model of drug-induced AKI.

As shown in Figures 3B and S24, the fluorescence of the main organs was unchanged after the injection of **FDOCl-22** via the tail vein of healthy mice. However, the fluorescence signal in the kidney of the AKI mouse model was clearly enhanced (Figure 3C). Given that **FDOCl-22** is only activated by HOCl, these experimental results indicate that HOCl concentration is closely correlated with drug-induced AKI, which was also found by Zhang et al. in their recent report.[27] All of the data suggest that HOCl could be used as a specific biomarker for the early detection of drug-induced AKI.

The same cisplatin-induced AKI mouse model was also used to evaluate PA imaging. As shown in Figure 3D, PA signals in the kidney of cisplatin-induced (20 mg/kg, 48 h) AKI mice became detectable at 10 min and then gradually increased in intensity within 40 min after injection of **FDOCl-22**. However, PA signals in the kidney of healthy mice were unchanged, even 40 min after injection of **FDOCl-22** (Figure S25). These data illustrated that the PA imaging results were consistent with those from fluorescence imaging. **FDOCl-22** could therefore be used for the diagnosis of drug-induced AKI using dual-modality NIRF and PA imaging.

Dual-Modality Detection of Early-Stage Cisplatin-Induced AKI Using the HOCl-Activated Probe FDOCl-22. Encouraged by its performance in the AKI mouse model, we investigated the potential of **FDOCl-22** for the detection of cisplatin-induced AKI in its early stage by dual-modality imaging. Sixteen mouse models were constructed with different degrees of renal injury by varying the intraperitoneal dose of cisplatin (0, 10, 20, and 40 mg/kg) and maintaining for different time periods (12, 24, 48, and 72 h). Forty minutes after intravenous injection of **FDOCl-22**, the kidneys were harvested from the mice for fluorescence imaging. As shown in Figure 4A, the fluorescence signal increased with both cisplatin dose and duration. A significant difference was observed at the right part of the red solid line compared with the control group (average fluorescence intensity output of the group is shown in the right column of Figure 4A), suggesting the renal injury in these models. To confirm and evaluate the level of renal injury, four mouse models (Nos. 7, 10, 11, and 15 in Figure 4A) were selected for comparison with commercial methods (Table S2). Blood urea nitrogen (BUN), serum creatinine (CREA), and uric acid (UA) were determined using commercial assays. As shown in Figure 4B, for models 11 and 15, all three indicators exceeded the normal range, indicating that renal injury in these two models could be detected using the commercial methods. However, for models 7 and 10, which were diagnosed as AKI using **FDOCl-22** (Figure 4A), no significant differences were detected using the three indicators compared to normal, indicating that commercial assays could not identify the early renal injury. These results confirmed that real-time imaging using **FDOCl-22** could identify drug-induced AKI at least 24 h earlier than commercial assays in the mouse model with the same drug dosage (20 mg/kg) or with a lower dosage (10 mg/kg) after the same stimulation time (48 h). TNF-α immunostaining analysis of the mouse model (10 mg/kg, 48 h) was also conducted to verify the accuracy of **FDOCl-22** for detecting early-stage drug-induced AKI. As we expected, the severity of kidney inflammation induced by low-dosage cisplatin was significantly higher than in healthy or LC pretreated mice (Figure S26). The results illustrated that **FDOCl-22** could be used as a tool for the detection of cisplatin-induced AKI in the early stage.

Finally, PA imaging was carried out *in situ* in the above two early-stage AKI mouse models after injection of **FDOCl-22**. PA images of the kidneys were recorded at 0 and 40 min. As shown in Figure 4C,D, the PA signals in the kidneys were enhanced 40 min after intravenous injection of **FDOCl-22**. In general, the HOCl-activated probe, **FDOCl-22**, was more sensitive for imaging of cisplatin-induced AKI in its earlier stage than the clinical methods, irrespective of drug stimulation time or dosage (Figure 4E).

CONCLUSIONS

In summary, we report a distinct activatable probe **FDOCl-22** containing an ethylene glycol chain and a MB fluorophore as the signal output unit for the detection of early-stage drug-induced AKI. The ethylene glycol chain guarantees that the **FDOCl-22** can be completely soluble in water without requiring any organic cosolvent (Table S1) and mainly through renal metabolism *in vivo* due to its high hydro-

https://dx.doi.org/10.1021/acssensors.0c00640
ACS Sens. 2020, 5, 2457−2466

philicity.[41,42] Especially, **FDOCl-22** released MB when reaction with HOCl and displayed remarkable changes of both fluorescence emission and absorption. Thus, **FDOCl-22** could be used for the identification of HOCl by dual-modality imaging (NIRF and PA imaging) *in vivo*, which could improve the accuracy of detection. This makes **FDOCl-22** an ideal probe for further biological application. Using **FDOCl-22** as a tool, we identified the presence of HOCl during cell apoptosis in drug-induced AKI for the first time. Moreover, **FDOCl-22** could perform dual-modality detection of AKI in the early stage by NIRF and PA imaging, irrespective of drug stimulation time or dosage. **FDOCl-22** thus has great potential for monitoring of kidney injury diseases and drug screening in clinical research. Efforts are ongoing to realize the clinical application of **FDOCl-22** and related derivatives.

EXPERIMENTAL SECTION

Preparation of Probes and Analytes. Stock solutions of **FDOCl-22** and **FDOCl-21** (1 mM) were prepared in deionized water and ethanol, respectively, and then diluting with phosphate-buffered solution (PBS, 10 mM, pH 7.4) to the test concentration. The test solutions were shaken well and placed at room temperature before recording the spectra. Other analytes were prepared in ddH_2O according to our reported procedure and details are as follows.[33,36] HOCl was obtained from a 14.5% NaOCl solution. H_2O_2 was diluted from a 30% solution. Hydroxyl radical ($^{\bullet}OH$) was generated by Fenton reaction ($H_2O_2/FeCl_2$ = 1:10), and the concentration of $^{\bullet}OH$ was equal to the concentration of H_2O_2. *tert*-Butyl hydroperoxide (TBHP) was obtained from 70% TBHP solution in ddH_2O. $ROO^{\bullet}$ was prepared by dissolving 2,2′-azobis(2-amidinopropane) dihydrochloride in ddH_2O. NO was prepared by dissolving sodium nitroferricyanide(III) dihydrate (SNP) in ddH_2O. O_2^- was prepared by dissolving potassium superoxide (KO_2) in DMSO. $ONOO^-$ was prepared using 3-morpholinosydnonimine hydrochloride. *t*-$BuOO^{\bullet}$ was prepared by adding TBHP in the presence of 10 equiv of ferrous chloride and the concentration of *t*-$BuOO^{\bullet}$ was equal to the TBHP concentration.

Cisplatin-Induced Acute Kidney Injury. Cisplatin was dissolved in PBS (10 mM, pH 7.4). F1 mice were intraperitoneally preinjected with different doses of cisplatin for different times, then i.v. injected with **FDOCl-22** (200 μL, 0.5 mM). Then, all of the mice were anesthetized and performed surgical procedure to expose organs. Imaging was observed using Bruker *in vivo* imaging system (*In Vivo* Xtreme) with a Xe lamp as an excitation source.

ASSOCIATED CONTENT

Supporting Information

The Supporting Information is available free of charge at https://pubs.acs.org/doi/10.1021/acssensors.0c00640.

Synthesis and characteristics of the probes, general method and equipment, and additional tables and figures (PDF)

AUTHOR INFORMATION

Corresponding Authors

Peng Wei − *College of Chemistry, Chemical Engineering and Biotechnology, Donghua University, Shanghai 201620, China*; Email: weipeng@dhu.edu.cn

Tao Yi − *Department of Chemistry, Fudan University, Shanghai 200438, China; College of Chemistry, Chemical Engineering and Biotechnology, Donghua University, Shanghai 201620, China*; orcid.org/0000-0002-3309-8556; Email: yitao@fudan.edu.cn

Authors

Lingyan Liu − *Department of Chemistry, Fudan University, Shanghai 200438, China*

Liping Jiang − *State Key Laboratory of Molecular Engineering of Polymers, Department of Macromolecular Science, Fudan University, Shanghai 200438, China*

Wei Yuan − *Department of Chemistry, Fudan University, Shanghai 200438, China*

Zhongkuan Liu − *Department of Chemistry, Fudan University, Shanghai 200438, China*

Dongya Liu − *Department of Chemistry, Fudan University, Shanghai 200438, China*

Xinyu Zhang − *School of Public Health, Hongqiao International Institute of Medicine, Shanghai Jiao Tong University School of Medicine, Shanghai 200025, China*

Complete contact information is available at: https://pubs.acs.org/10.1021/acssensors.0c00640

Author Contributions

The manuscript was written through contributions of all authors. All authors have given approval to the final version of the manuscript.

Notes

The authors declare no competing financial interest.

ACKNOWLEDGMENTS

This work is financially supported by the National Natural Science Foundation of China (21877013 and 21671043).

ABBREVIATIONS USED

AKI, acute kidney injury; HOCl, hypochlorous acid; PBS, phosphate-buffered saline; CREA, serum creatinine; BUN, blood urea nitrogen; NIRF, near-infrared fluorescence, photoacoustic

REFERENCES

(1) Jha, V.; Garcia-Garcia, G.; Iseki, K.; Li, Z.; Naicker, S.; Plattner, B.; Saran, R.; Wang, A. Y.-M.; Yang, C.-W. Chronic kidney disease: global dimension and perspectives. *Lancet* **2013**, *382*, 260−272.

(2) Perazella, M. A.; Coca, S. G. Three feasible strategies to minimize kidney injury in'incipient AKI'. *Nat. Rev. Nephrol.* **2013**, *9*, 484−490.

(3) Schrier, R. W.; Wang, W. Acute renal failure and sepsis. *N. Engl. J. Med.* **2004**, *351*, 159−169.

(4) Chawla, L. S.; Eggers, P. W.; Star, R. A.; Kimmel, P. L. Acute kidney injury and chronic kidney disease as interconnected syndromes. *N. Engl. J. Med.* **2014**, *371*, 58−66.

(5) Ueda, N.; Kaushal, G. P.; Shah, S. V. Apoptotic mechanisms in acute renal failure. *Am. J. Med.* **2000**, *108*, 403−415.

(6) Kellum, J. A.; Prowle, J. R. Paradigms of acute kidney injury in the intensive care setting. *Nat. Rev. Nephrol.* **2018**, *14*, 217−230.

(7) Sasaki, D.; Yamada, A.; Umeno, H.; Kurihara, H.; Nakatsuji, S.; Fujihira, S.; Tsubota, K.; Ono, M.; Moriguchi, A.; Watanabe, K.; et al. Comparison of the course of biomarker changes and kidney injury in a rat model of drug-induced acute kidney injury. *Biomarkers* **2011**, *16*, 553−566.

(8) Wang, X.; Lewis, J.; Appel, L.; Cheek, D.; Contreras, G.; Faulkner, M.; Feldman, H.; Gassman, J.; Lea, J.; Kopple, J.; et al. Validation of creatinine-based estimates of GFR when evaluating risk factors in longitudinal studies of kidney disease. *J. Am. Soc. Nephrol.* **2006**, *17*, 2900−2909.

(9) Galgamuwa, R.; Hardy, K.; Dahlstrom, J. E.; Blackburn, A. C.; Wium, E.; Rooke, M.; Cappello, J. Y.; Tummala, P.; Patel, H. R.; Chuah, A.; et al. Dichloroacetate prevents cisplatin-induced

nephrotoxicity without compromising cisplatin anticancer properties. *J. Am. Soc. Nephrol.* **2016**, *27*, 3331−3344.
(10) Sharfuddin, A. A.; Molitoris, B. A. Pathophysiology of ischemic acute kidney injury. *Nat. Rev. Nephrol.* **2011**, *7*, 189−200.
(11) Grigoryev, D. N.; Liu, M.; Hassoun, H. T.; Cheadle, C.; Barnes, K. C.; Rabb, H. The local and systemic inflammatory transcriptome after acute kidney injury. *J. Am. Soc. Nephrol.* **2008**, *19*, 547−558.
(12) Bonventre, J. V.; Yang, L. Cellular pathophysiology of ischemic acute kidney injury. *J. Clin. Invest.* **2011**, *121*, 4210−4221.
(13) Ren, M.; Zhou, K.; He, L.; Lin, W. Mitochondria and lysosome-targetable fluorescent probes for HOCl: recent advances and perspectives. *J. Mater. Chem. B* **2018**, *6*, 1716−1733.
(14) Bae, J.; McNamara, L. E.; Nael, M. A.; Mahdi, F.; Doerksen, R. J.; Bidwell, G. L., 3rd; Hammer, N. I.; Jo, S. Nitroreductase-triggered activation of a novel caged fluorescent probe obtained from methylene blue. *Chem. Commun.* **2015**, *51*, 12787−12790.
(15) Rong, G.; Corrie, S. R.; Clark, H. A. In Vivo Biosensing: Progress and Perspectives. *ACS Sensors* **2017**, *2*, 327−338.
(16) New, E. J. Harnessing the Potential of Small Molecule Intracellular Fluorescent Sensors. *ACS Sensors* **2016**, *1*, 328−333.
(17) Wang, X.; Li, P.; Ding, Q.; Wu, C.; Zhang, W.; Tang, B. Illuminating the Function of the Hydroxyl Radical in the Brains of Mice with Depression Phenotypes by Two-Photon Fluorescence Imaging. *Angew. Chem., Int. Ed.* **2019**, *58*, 4674−4678.
(18) Wang, X.; Li, P.; Ding, Q.; Wu, C.; Zhang, W.; Tang, B. Observation of Acetylcholinesterase in Stress-Induced Depression Phenotypes by Two-Photon Fluorescence Imaging in the Mouse Brain. *J. Am. Chem. Soc.* **2019**, *141*, 2061−2068.
(19) Lee, S.; Park, K.; Kim, K.; Choi, K.; Kwon, I. C. Activatable imaging probes with amplified fluorescent signals. *Chem. Commun.* **2008**, *36*, 4250−4260.
(20) Kobayashi, H.; Choyke, P. L. Target-cancer-cell-specific activatable fluorescence imaging probes: rational design and in vivo applications. *Acc. Chem. Res.* **2010**, *44*, 83−90.
(21) Zhao, X.; Ji, C.; Ma, L.; Wu, Z.; Cheng, W.; Yin, M. An Aggregation-Induced Emission-Based "Turn-On" Fluorescent Probe for Facile Detection of Gaseous Formaldehyde. *ACS Sensors* **2018**, *3*, 2112−2117.
(22) Huang, J.; Li, J.; Lyu, Y.; Miao, Q.; Pu, K. Molecular optical imaging probes for early diagnosis of drug-induced acute kidney injury. *Nat. Mater.* **2019**, *18*, 1133−1143.
(23) Cheng, P.; Chen, W.; Li, S.; He, S.; Miao, Q.; Pu, K. Fluoro-Photoacoustic Polymeric Renal Reporter for Real-Time Dual Imaging of Acute Kidney Injury. *Adv. Mater.* **2020**, *32*, No. 1908530.
(24) Huang, J.; Lyu, Y.; Li, J.; Cheng, P.; Jiang, Y.; Pu, K. A Renal-Clearable Duplex Optical Reporter for Real-Time Imaging of Contrast-Induced Acute Kidney Injury. *Angew. Chem., Int. Ed.* **2019**, *58*, 17796−17804.
(25) Huang, J.; Xie, C.; Zhang, X.; Jiang, Y.; Li, J.; Fan, Q.; Pu, K. Renal-clearable Molecular Semiconductor for Second Near-Infrared Fluorescence Imaging of Kidney Dysfunction. *Angew. Chem., Int. Ed.* **2019**, *58*, 15120−15127.
(26) Lv, Y.; Cheng, D.; Su, D.; Chen, M.; Yin, B.-C.; Yuan, L.; Zhang, X.-B. Visualization of oxidative injury in the mouse kidney using selective superoxide anion fluorescent probes. *Chem. Sci.* **2018**, *9*, 7606−7613.
(27) Wang, J.; Cheng, D.; Zhu, L.; Wang, P.; Liu, H.-W.; Chen, M.; Yuan, L.; Zhang, X.-B. Engineering dithiobenzoic acid lactone-decorated Si-rhodamine as a highly selective near-infrared HOCl fluorescent probe for imaging drug-induced acute nephrotoxicity. *Chem. Commun.* **2019**, *55*, 10916−10919.
(28) Louie, A. Multimodality imaging probes: design and challenges. *Chem. Rev.* **2010**, *110*, 3146−3195.
(29) Meng, L.; Wu, Y.; Yi, T. A ratiometric fluorescent probe for the detection of hydroxyl radicals in living cells. *Chem. Commun.* **2014**, *50*, 4843−4845.
(30) Wen, Y.; Liu, K.; Yang, H.; Li, Y.; Lan, H.; Liu, Y.; Zhang, X.; Yi, T. A highly sensitive ratiometric fluorescent probe for the detection of cytoplasmic and nuclear hydrogen peroxide. *Anal. Chem.* **2014**, *86*, 9970−9976.
(31) Wen, Y.; Liu, K.; Yang, H.; Liu, Y.; Chen, L.; Liu, Z.; Huang, C.; Yi, T. Mitochondria-directed fluorescent probe for the detection of hydrogen peroxide near mitochondrial DNA. *Anal. Chem.* **2015**, *87*, 10579−10584.
(32) Wen, Y.; Xue, F.; Lan, H.; Li, Z.; Xiao, S.; Yi, T. Multicolor imaging of hydrogen peroxide level in living and apoptotic cells by a single fluorescent probe. *Biosens. Bioelectron.* **2017**, *91*, 115−121.
(33) Wei, P.; Yuan, W.; Xue, F.; Zhou, W.; Li, R.; Zhang, D.; Yi, T. Deformylation reaction-based probe for in vivo imaging of HOCl. *Chem. Sci.* **2018**, *9*, 495−501.
(34) Cao, C.; Wei, P.; Li, R.; Zhong, Y.; Li, X.; Xue, F.; Shi, Y.; Yi, T. Ribosomal RNA-selective light-up fluorescent probe for rapidly imaging the nucleolus in live cells. *ACS Sensors* **2019**, *4*, 1409−1416.
(35) Wei, P.; Liu, L.; Yuan, W.; Yang, J.; Li, R.; Yi, T. A fluorescent probe operating under weak acidic conditions for the visualization of HOCl in solid tumors in vivo. *Sci. China: Chem.* **2020**, *63*, 1153−1158.
(36) Wei, P.; Liu, L.; Wen, Y.; Zhao, G.; Xue, F.; Yuan, W.; Li, R.; Zhong, Y.; Zhang, M.; Yi, T. Release of amino-or carboxy-containing compounds triggered by HOCl: application for imaging and drug design. *Angew. Chem., Int. Ed.* **2019**, *58*, 4547−4551.
(37) Song, K. H.; Stein, E. W.; Margenthaler, J. A.; Wang, L. V. Noninvasive photoacoustic identification of sentinel lymph nodes containing methylene blue in vivo in a rat model. *J. Biomed. Opt.* **2008**, *13*, No. 054033.
(38) Zeng, Q.; Zhang, R.; Zhang, T.; Xing, D. H2O2-responsive biodegradable nanomedicine for cancer-selective dual-modal imaging guided precise photodynamic therapy. *Biomaterials* **2019**, *207*, 39−48.
(39) Zackrisson, S.; van de Ven, S.; Gambhir, S. Light in and sound out: emerging translational strategies for photoacoustic imaging. *Cancer. Res.* **2014**, *74*, 979−1004.
(40) Wang, L. V.; Hu, S. Photoacoustic tomography: in vivo imaging from organelles to organs. *Science* **2012**, *335*, 1458−1462.
(41) Wang, Y.; Meng, Y.; Wang, S.; Li, C.; Shi, W.; Chen, J.; Wang, J.; Huang, R. Direct solvent-derived polymer-coated nitrogen-doped carbon nanodots with high water solubility for targeted fluorescence imaging of glioma. *Small* **2015**, *11*, 3575−3581.
(42) Izzedine, H.; Perazella, M. A. Anticancer drug-induced acute kidney injury. *Kidney Int. Rep.* **2017**, *2*, 504−514.
(43) Uranga, J.; Mujika, J. I.; Grande-Aztatzi, R.; Matxain, J. M. Oxidation of acid, base, and amide side-chain amino acid derivatives via hydroxyl radical. *J. Phys. Chem. B.* **2018**, *122*, 4956−4971.
(44) Deng, T.; Wang, X.; Wu, S.; Hu, S.; Liu, W.; Chen, T.; Yu, Z.; Xu, Q.; Liu, F. A new FRET probe for ratiometric fluorescence detecting mitochondria-localized drug activation and imaging endogenous hydroxyl radicals in zebrafish. *Chem. Commun.* **2020**, *56*, 4432−4435.
(45) Ozkok, A.; Edelstein, C. L. Pathophysiology of cisplatin-induced acute kidney injury. *BioMed. Res. Int.* **2014**, *2014*, 967826−967843.
(46) Sureshbabu, A.; Ryter, S. W.; Choi, M. E. Oxidative stress and autophagy: crucial modulators of kidney injury. *Redox. Biol.* **2015**, *4*, 208−214.
(47) Circu, M. L.; Aw, T. Y. Reactive oxygen species, cellular redox systems, and apoptosis. *Free Radical Biol. Med.* **2010**, *48*, 749−762.
(48) Wynn, T. A.; Chawla, A.; Pollard, J. W. Macrophage biology in development, homeostasis and disease. *Nature* **2013**, *496*, 445−455.
(49) Whiteman, M.; Hooper, D. C.; Scott, G. S.; Koprowski, H.; Halliwell, B. Inhibition of hypochlorous acid-induced cellular toxicity by nitrite. *Proc. Natl. Acad. Sci. U.S.A.* **2002**, *99*, 12061−12066.
(50) Feng, H.; Zhang, Z.; Meng, Q.; Jia, H.; Wang, Y.; Zhang, R. Rapid response fluorescence probe enabled in vivo diagnosis and assessing treatment response of hypochlorous acid-mediated rheumatoid arthritis. *Adv. Sci.* **2018**, *5*, No. 1800397.
(51) Sugiyama, S.; Kugiyama, K.; Aikawa, M.; Nakamura, S.; Ogawa, H.; Libby, P. Hypochlorous acid, a macrophage product, induces endothelial apoptosis and tissue factor expression: involvement of

https://dx.doi.org/10.1021/acssensors.0c00640
ACS Sens. 2020, 5, 2457−2466

myeloperoxidase-mediated oxidant in plaque erosion and thrombogenesis. *Arterioscler., Thromb., Vasc. Biol.* **2004**, *24*, 1309−1314.
(52) Englert, R. P.; Shacter, E. Distinct modes of cell death induced by different reactive oxygen species amino acyl chloramines mediate hypochlorous acid-induced apoptosis. *J. Biol. Chem.* **2002**, *277*, 20518−20526.
(53) Davis, C. A.; Nick, H. S.; Agarwal, A. Manganese superoxide dismutase attenuates cisplatin-induced renal injury: importance of superoxide. *J. Am. Soc. Nephrol.* **2001**, *12*, 2683−2690.

https://dx.doi.org/10.1021/acssensors.0c00640
ACS Sens. 2020, 5, 2457−2466